# Conjugate heat transfer shape optimization of internal cooling systems using continuous adjoint in OpenFOAM

K.T. Gkaragkounis, E.M. Papoutsis-Kiachagias, K.C. Giannakoglou

*Lab. of Thermal Turbomachines, Parallel CFD & Optimization Unit, School of Mechanical Engineering*
*National Technical University of Athens 9, Iroon Polytechniou, 15780, Athens, Greece*

## 1. Introduction

Shape optimization of internal cooling systems has been performed either using evolutionary algorithms (1; 2) or gradient-based methods, with the latter mostly relying on adjoint approaches (3; 4; 5; 6; 7; 8). Adjoint methods are widely used, since they can compute the gradients of objective and constraint functions at a cost which does not scale with the number of design variables. However, adjoint methods for the shape optimizations of internal cooling systems have mostly been developed and used separately for the fluid flow and the solid heat conduction PDEs. Recently, in (9), the continuous adjoint for Conjugate Heat Transfer (CHT) problems with compressible fluid flows was presented without though differentiating the turbulence model PDEs. Then, the continuous adjoint method to CHT problems for incompressible turbulent flows was derived in (10) by the authors of this paper. In contrast to (9), the method proposed in (10) overcomes the "frozen turbulence assumption" by including variations in the Spalart-Allmaras turbulence model in the development of the adjoint equations and taking into consideration grid sensitivities.

This paper investigates the trade-off between optimizing the effectiveness of cooling systems and minimizing the total pressure losses between the inlet and outlet of the cooling duct. An adjoint-assisted optimization algorithm, able to solve constrained problems using SQP and line-search (11), has been programmed and is used in a 2D CHT problem to perform various optimizations and investigate the aforementioned trade-offs. In order to compute the gradients of the objective and constraint functions, the continuous adjoint method for CHT problems with turbulent flows, developed in (10) by the current authors, is used. Additionally, the internal cooling of a solid body cooled through fluid flowing in a 3D U-Bend channel is investigated; this case is met in the literature as a simplified cooling system of internal combustion engines (8). Optimizations are carried out for an objective function penalizing increased solid temperature values, as in (10), and a new function expressing the heat flux crossing the Fluid-Solid Interface (FSI) towards the coolant. To parameterize the geometries and deform the meshes during the optimization in both 2D and 3D cases, a volumetric B-Splines morpher is used.

In section 2, the primal and adjoint equations for CHT problems, along with the expression of the sensitivity derivatives (SDs) are briefly presented. In sections 3 and 4, the volumetric B-Splines morpher and the optimization algorithm are discussed. In section 5, 2D and 3D cases are studied. The methods used in this paper are programmed in the open-source CFD toolbox OpenFOAM, version 2.3.1. The line-search based optimization algorithm is driven by an OpenFOAM executable which is responsible for the solution of the primal and adjoint equations, parameterization, SDs computation, update of the design variables and, finally, mesh movement. To do so, the CHT solver (among others) is incorporated in the optimization algorithm as a class object, which is constructed at run-time, depending on the input provided by the user.

## 2. Primal and Adjoint CHT Equations

Let $\Omega^F$ be the fluid and $\Omega^S$ the solid domain, separated by the FSI $\overline{S}$; this is occasionally denoted as $\bar{S}_F$ or $\bar{S}_S$, depending on whether it is seen from the fluid or solid domain, respectively, see fig. 1.

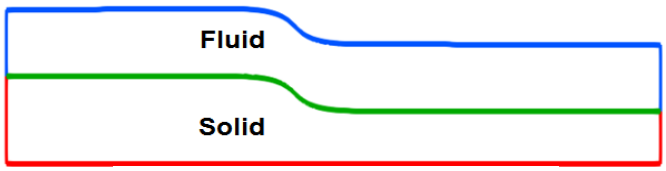


**Figure 1: An example of a 2D CHT problem.**

The steady flow is governed by the incompressible Reynolds-Averaged Navier Stokes equations, with closure effected by the one-equation Spalart-Allmaras turbulence model (12). In Table 1, the primal CHT equations as well as the corresponding adjoint ones, arising by following the mathematical development presented in detail in (10), are summarized. Eqs. (1) and (2) stand for the continuity and momentum equations, eqs. (3) and (6) govern the heat transfer through the FSI and eq. (5) is the Hamilton-Jacobi equation solved to obtain the distance field Δ required by the turbulence model eq. (4). In these equations, $v_i, p, \tilde{\nu}$ are the velocity components, the static pressure divided by the constant fluid density $\rho_F$ and the turbulence model variable and $T^D$ (D=F,S) are the temperatures in $\Omega^F$ and $\Omega^S$. Also, $\nu$ stands for the kinematic viscocity, $\tau_{ij} = (\nu + \nu_t)\left(\frac{\partial v_i}{\partial x_j} + \frac{\partial v_j}{\partial x_i}\right)$ are the stresses, $\nu_t = f_{v1}\tilde{\nu}$ is the eddy viscocity, $k^F = \rho_F c_p \alpha_{eff} = \rho_F c_p \left(\frac{\nu}{Pr} + \frac{\tilde{\nu}}{Pr_t}\right)$ and $k^S$ are the thermal conductivities in the two domains, $c_p$ is the specific heat transfer coefficient under constant pressure and $Pr$ and $Pr_t$ the bulk and turbulent Prandtl numbers. Repeated indices imply summation. Terms $\mathcal{P}(\tilde{\nu}), \mathcal{D}(\tilde{\nu}), C_{b1}, f_{v1}, f_{v2}, \tilde{S}, \sigma, C_{b2}, C_{w1}, f_w$ can be found in (12; 13).

Assuming that the boundary $S_F$ of $\Omega^F$ is decomposed into $S_{F,I}, S_{F,O}, \overline{S}_F$ and $S_{F,W}$, standing for the inlet, outlet, FSI and non-FSI walls, respectively, the boundary conditions (BCs) imposed along $S_{F,I}$ are zero-Neumann conditions for $p$ and Dirichlet conditions for all other flow variables. Also, along $S_{F,O}$, the pressure is fixed and zero Neumann conditions are imposed on $v_i$, $T^F$ and $\tilde{\nu}$. Along $S_{F,W}$ and $\overline{S}_F$, a no-slip

condition on the velocity and a zero-Neumann condition on $p$ are imposed. $S_{F,W}$ is considered to be adiabatic. Moreover, the $\Omega^S$ boundaries $S_S$ are decomposed into $S_{S,D}, S_{S,Fl}$ and $\overline{S}_S$; along $S_{S,D}$ and $S_{S,Fl}$, Dirichlet boundary conditions on temperature and heat-flux distributions are imposed, respectively.

Functions used in this paper, either as objectives or constraints, are defined over $\Omega^S$, $\bar{S}^F$, $S_{F,I}$ and $S_{F,O}$ respectively as $J_{\Omega^S} = \int_{\Omega^S} j_\Omega d\Omega$, $J_{\bar{S}} = \int_{\bar{S}} j_{\bar{S}} dS$ and $J_{S_{F,I,O}} = \int_{S_{F,I} \cup S_{F,O}} j_{S_{F,I,O}} dS$.

Following the mathematical development presented in detail in (10), the adjoint continuity, momentum, turbulence model, Hamilton-Jacobi and $\Omega^F$ and $\Omega^S$ heat transfer PDEs, listed as eqs. (7)-(12) in Table 1, arise. In those equations, variables $q, u_i, \tilde{\nu}_a, \Delta_a, T_a^D$ stand for the adjoint pressure, velocities, turbulence model variable, distance and temperature fields. Also, $\tau_{ij}^a = (\nu + \nu_t)(\frac{\partial u_i}{\partial x_j} + \frac{\partial u_j}{\partial x_i})$ stands for the adjoint stress tensor, $e_{ijk}$ is the Levi-Civita symbol and $C_{\tilde{\nu}}$, $C_Y$ and $Y$ can be found in (14). A detailed presentation of the adjoint boundary conditions can be found in (10; 14).

| **Primal CHT PDEs** | **Adjoint CHT PDEs** |
|---|---|
| $R^p = -\frac{\partial v_j}{\partial x_j} = 0$ (1) | $R^p = \frac{\partial u_j}{\partial x_j} = 0$ (7) |
| $R_i^v = v_j \frac{\partial v_i}{\partial x_j} - \frac{\partial \tau_{ij}}{\partial x_j} + \frac{\partial p}{\partial x_i} = 0,\ i = 1,2(,3)$ (2) | $R_i^u = u_j \frac{\partial v_j}{\partial x_i} - \frac{\partial (v_j u_i)}{\partial x_j} - \frac{\partial \tau_{ij}^a}{\partial x_j} + \frac{\partial q}{\partial x_i} + \rho_F c_p T_a^F \frac{\partial T^F}{\partial x_i} + \rho_F T_a^F v_k \frac{\partial v_k}{\partial x_i}$ $- \rho_F v_i v_k \frac{\partial T_a^F}{\partial x_k} + \tilde{\nu}_a \frac{\partial \tilde{\nu}}{\partial x_i} - \frac{\partial}{\partial x_l}\left(\tilde{\nu}_a \tilde{\nu} \frac{C_Y}{Y} e_{mjk} \frac{\partial v_k}{\partial x_j} e_{mli}\right) = 0$ (8) |
| $R_F^T = \rho_F v_j c_p \frac{\partial T^F}{\partial x_j} + \rho_F \frac{v_j}{2} \frac{\partial v_k^2}{\partial x_j} - \frac{\partial}{\partial x_j}\left(k^F \frac{\partial T^F}{\partial x_j}\right) = 0$ (3) | $R_F^{T_a} = -\frac{\partial (v_j T_a^F)}{\partial x_j} - \frac{\partial}{\partial x_j}\left(\alpha_{eff} \frac{\partial T_a^F}{\partial x_j}\right) = 0$ (9) |
| $R^{\tilde{\nu}} = v_j \frac{\partial \tilde{\nu}}{\partial x_j} - \frac{\partial}{\partial x_j}\left[\left(\nu + \frac{\tilde{\nu}}{\sigma}\right)\frac{\partial \tilde{\nu}}{\partial x_j}\right] - \frac{C_{b2}}{\sigma}\left(\frac{\partial \tilde{\nu}}{\partial x_j}\right)^2$ $- \tilde{\nu}\mathcal{P}(\tilde{\nu}) + \tilde{\nu}\mathcal{D}(\tilde{\nu}) = 0$ (4) | $R^{\tilde{\nu}_a} = -v_j \frac{\partial \tilde{\nu}_a}{\partial x_j} - \frac{\partial}{\partial x_j}\left[\left(\nu + \frac{\tilde{\nu}}{\sigma}\right)\frac{\partial \tilde{\nu}_a}{\partial x_j}\right] + \frac{1}{\sigma}\frac{\partial \tilde{\nu}_a}{\partial x_j}\frac{\partial \tilde{\nu}}{\partial x_j} + \tilde{\nu}_a \tilde{\nu} C_{\tilde{\nu}}(\tilde{\nu}, v_i) - (\mathcal{P} - \mathcal{D})\tilde{\nu}_a$ $+ 2\frac{C_{b2}}{\sigma}\frac{\partial}{\partial x_j}\left(\tilde{\nu}_a \frac{\partial \tilde{\nu}}{\partial x_j}\right) + \left[\frac{\partial u_i}{\partial x_j}\left(\frac{\partial v_i}{\partial x_j} + \frac{\partial v_j}{\partial x_i}\right) + \rho_F \frac{c_p}{Pr_t}\frac{\partial T_a^F}{\partial x_j}\frac{\partial T^F}{\partial x_j}\right]\frac{\delta \nu_t}{\delta \tilde{\nu}} = 0$ (10) |
| $R^\Delta = \frac{\partial (c_j \Delta)}{\partial x_j} - \Delta \frac{\partial^2 \Delta}{\partial x_j^2} - 1 = 0,\ c_j = \frac{\partial \Delta}{\partial x_j}$ (5) | $R^{\Delta_a} = -2\frac{\partial}{\partial x_j}\left(\Delta_a \frac{\partial \Delta}{\partial x_j}\right) + \tilde{\nu}_a \tilde{\nu} C_\Delta = 0$ (11) |
| $R_S^T = -\frac{\partial}{\partial x_j}\left[k^S \frac{\partial T^S}{\partial x_j}\right] = 0$ (6) | $R_S^{T_a} = -\frac{\partial}{\partial x_j}\left(k^S \frac{\partial T_a^S}{\partial x_j}\right) + \frac{\partial j_\Omega}{\partial T^S} = 0$ (12) |

**Table 1: Primal and adjoint PDEs in a CHT problem involving a turbulent flow. Equations in the first row are solved over $\Omega^F$ and those in the second row over $\Omega^S$.**

| Primal | Adjoint |
|---|---|
| $T^F\|_{\bar{S}_F} = T^S\|_{\bar{S}_S}$ | $\rho^F T_a^F\|_{\bar{S}_F} + J_1\|_{\bar{S}} = \rho^S T_a^S\|_{\bar{S}_S}$ |
| $k^F\left(\frac{\partial T^F}{\partial x_j} n_j\right)_{\bar{S}_F} = -k^S\left(\frac{\partial T^S}{\partial x_j} n_j\right)_{\bar{S}_S}$ | $k^F \frac{\partial T_a^F}{\partial n}\|_{\bar{S}_F} + J_2\|_{\bar{S}} = -k^S \frac{\partial T_a^S}{\partial n}\|_{\bar{S}_S}$ |

**Table 2: Primal and adjoint conditions imposed along the FSI.**

Considering the primal conditions along both sides of the FSI, heat-flux conservation and temperature equality conditions are imposed, see Table 2. The adjoint FSI conditions are similar to the primal ones, with terms $J_i|_{\bar{S}}, i = 1,2$ being contributions from objective functions along the FSI, such as the total heat flux crossing it from $\Omega^S$ to $\Omega^F$, see eq. (17).

Since eqs. (1),(2),(4),(5) do not depend on either $T^F$ or $T^S$, eqs. (3) and (6) can be solved separately, after the solution of the remaining flow equations. On the other hand, eqs. (9) and (12) can be solved prior to the remaining adjoint equations, since they do not include any of $u_i$, $q$ or $\tilde{\nu}$.

The expression of the SDs for $\boldsymbol{J_{\Omega^S}}$ read

$$\frac{\delta J_{\Omega^S}}{\delta b_n} = \int_{\Omega^S} j_\Omega \frac{\partial}{\partial x_k}\left(\frac{\delta x_k}{\delta b_n}\right) d\Omega + \int_{S_{F,W}\cup\bar{S}_F} k^F T_a^F \frac{\partial T^F}{\partial x_j}\frac{\delta n_j}{\delta b_n} dS + \int_{S_{S,FI}\cup\bar{S}_S} k^S T_a^S \frac{\partial T^S}{\partial x_j}\frac{\delta n_j}{\delta b_n} dS + \int_{\Omega^F} \Big[ -u_i v_j \frac{\partial v_i}{\partial x_k} - \tau_{ij}^a \frac{\partial v_i}{\partial x_k} + u_i \frac{\partial \tau_{ij}}{\partial x_k} - u_j \frac{\partial p}{\partial x_k} + q\frac{\partial v_j}{\partial x_k} - \rho_F c_p T_a^F v_j \frac{\partial T^F}{\partial x_k} - \rho_F T_a^F v_j v_i \frac{\partial v_i}{\partial x_k} - k^F \frac{\partial T_a^F}{\partial x_j}\frac{\partial T^F}{\partial x_k} + T_a^F \frac{\partial}{\partial x_k}\left(k^F \frac{\partial T^F}{\partial x_j}\right) + \Theta_{M,jk}\Big] \frac{\partial}{\partial x_j}\left(\frac{\delta x_k}{\delta b_n}\right) d\Omega + \int_{\Omega^S} \left( -k^S \frac{\partial T_a^S}{\partial x_j}\frac{\partial T^S}{\partial x_k} + k^S T_a^S \frac{\partial^2 T^S}{\partial x_j \partial x_k}\right) \frac{\partial}{\partial x_j}\left(\frac{\delta x_k}{\delta b_n}\right) d\Omega \quad (13)$$

where $\Theta_{M,jk}$ is the contribution of the Spalart-Allmaras PDE to the SDs, see (10; 14). Concerning $J_{\bar{S}}$, a similar expression without the first term on the RHS of eq. (13) gives the adjoint sensitivities, while for $J_{S_{F,I,O}}$, the SDs expressions are given by the fourth term on the RHS of eq. (13) by omitting terms depending on $T^F$.

## 3. Volumetric B-Splines Morpher

During optimization, geometry parameterization is managed through a volumetric B-Splines morpher (15). One or more lattices of control points (CPs) are placed around or within the geometry and the CFD mesh points $x_i$ residing inside the control boxes are displaced simultaneously with the CPs. The parameterization reads

$$x_i = U_{k,pu}(u) V_{l,pv}(v) W_{m,pw}(w) b_i^{k,l,m} \quad (14)$$

where $b_i$ correspond to the x,y,z coordinates of the CPs, $U, V, W$ to the B-Splines basis-functions and $u, v, w$ to the parametric coordinates of the mesh points residing in the control boxes (15). An example of the parameterization is presented in fig. 2.

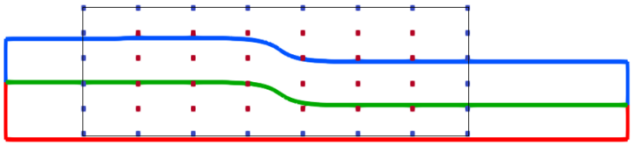

**Figure 2: Parameterization of the initial geometry of the 2D CHT problem. Blue CPs are still and red ones can be displaced. In this way, continuity of displacement at the morphing box (thin black line) boundaries is ensured.**

## 4. Optimization Algorithm

The optimization algorithm used in this paper can handle both constrained and unconstrained problems. In unconstrained problems, the update of the design variables $\mathbf{\Delta b_n}$ can be computed by means of a steepest descent (StD), conjugate gradient (CG) or Quasi-Newton (QN) method. In constrained problems with $\mathbf{N_c}$ equality constraints $\mathbf{C_i} = \mathbf{0}, \boldsymbol{i} \in [\mathbf{1}, \boldsymbol{N_c}]$, a Lagrangian $\mathbf{L} = \mathbf{J} + \boldsymbol{\lambda_i}\mathbf{C_i}$ is formed, with $\boldsymbol{\lambda_i}$ being the Lagrange multipliers and an SQP algorithm is used to satisfy the Karush–Kuhn–Tucker (KKT) conditions; to do so, the following system of equations is solved

$$\begin{bmatrix} \left[\frac{\delta^2 L}{\delta b_n \delta b_m}\right] & -\left[\frac{\delta C_i}{\delta b_n}\right]^T \\ \left[\frac{\delta C_i}{\delta b_n}\right] & [\emptyset] \end{bmatrix} \begin{bmatrix} \Delta b_n \\ \lambda_i \end{bmatrix} = - \begin{bmatrix} \frac{\delta J}{\delta b_m} \\ C_i \end{bmatrix}$$

to compute $\Delta b_n$ and update $\lambda_i$. The required Hessian $\left[\frac{\delta^2 L}{\delta b_n \delta b_m}\right]$ is approximated by the damped version of the BFGS method (11).

The use of the line-search method, Table 3, aims at computing an appropriate step length $a^k$ in order to scale $\Delta b_n$ and guarantee a sufficiently large change in the function $\varphi = J + \mu \sum_{i=1}^{N_c} |C_i|$, where, in the presence of constraints, $\mu$ is a penalty parameter updated in each optimization cycle to become equal to $max.|\lambda_i| + 2\delta$, in case $\mu < max.|\lambda_i| + \delta$, with $\delta > 0$ having a small constant value (11); in unconstrained problems, $\mu = 0$. At the *k*-th optimization cycle and before initializing the line-search loop of Table 3, $a^k$ is initialized with a constant value (equal to 1 for QN optimization methods) or is extrapolated from $a^{k-1}$. At each line-search iteration $l$ (not to exceed $N_{ls}$ in each optimization cycle), $a^k$ is updated either by multiplying it with a constant positive value smaller than 1 or by fitting a quadratic (in terms of $a^k$) polynomial to $\varphi$ (11). Once the Armijo condition

$$\varphi^l \leq \varphi^0 + c_1 a^k D\varphi_n^0 \Delta b_n$$

is satisfied (11), the line-search loop of Table 3 terminates. In the above expression, $\varphi^0$ and $D\varphi_n^0 \Delta b_n$ are computed before the start of the line-search loop of Table 3, with $D\varphi_n^0 \Delta b_n = \frac{\delta J}{\delta b_n} \Delta b_n - \mu \sum_{i=1}^{N_c} |C_i|$ for constrained problems or $D\varphi_n^0 \Delta b_n = \frac{\delta J}{\delta b_n} \Delta b_n$ for unconstrained ones and $c_1 < 1$ is a used-defined

positive constant (11). The optimization terminates when the KKT conditions are satisfied within an engineering accuracy or when the maximum number of optimization cycles has been reached.

**Optimization Algorithm:**

- Start from initial geometry $\boldsymbol{b}^0$
- Solve the primal equations
- Evaluate objective and constraint function(s)
- Solve the adjoint equations
- **For** k=1,2,3,…, $N_k$
  - Compute adjoint sensitivities
  - Compute $\Delta\boldsymbol{b}^k$ using StD/CG/QN or SQP
  - Update $\mu$ if needed
  - Compute $\varphi^{k,0} = J + \mu\sum_{i=1}^{N_c}|C_i|$ and directional derivative $D\varphi_n^0\Delta b_n = \frac{\delta J}{\delta b_n}\Delta b_n - \mu\sum_{i=1}^{N_c}|C_i|$
  - Initialize $a^k$
  - In constrained optimization, compute new values of $\lambda_i$ with the SQP method
  - **For** l=1,2,… $N_{ls}$ (l=1: Start of line-search)
    - Set $\boldsymbol{p}^k = a^k\Delta\boldsymbol{b}^k$ and $\boldsymbol{b}^k = \boldsymbol{b}^{k-1} + \boldsymbol{p}^k$
    - Update $\Omega^F$, $\Omega^S$ shapes and the corresponding meshes
    - Solve the primal equations
    - Compute $\varphi^{k,l}$
    - **If** $\varphi^{k,l} \leq \varphi^{k,0} + c_1\mathbf{D}\boldsymbol{\varphi}^{\boldsymbol{k,0}}\boldsymbol{p}^k$
      **End** of line-search
    - **Else**
      Update $a^k$
    - **End (if)**
  - **End (for)**
  - **If** termination criteria
    EXIT optimization loop
  - **End (If)**
  - Solve the adjoint equations
- **End** (**for**)

**Table 3: Optimization algorithm using the Armijo backtracking line-search method.**

## 5. CHT optimization cases

### 5.1 2D optimization case

Before proceeding to the 3D case(s), 2D constrained optimizations are presented; these are dealing with a solid body cooled by a fluid passing through an S-bend cooling channel located along one of the sides of $\Omega^S$ (practically lying above the side the shape of which should be designed, figs. 1,4). The coolant flow is turbulent ($y^+ < 1$) with Re=10000 entering with $T^F = 291.2K$, the rest of the non-FSI $\Omega^F$ boundaries are adiabatic and a constant temperature $T^S = 500K$ along the non-FSI $\Omega^S$ boundaries is considered. Also, $c_p = 4181\ J/K/kg$, $Pr = 0.1$, $Pr_t = 1$ and $k^S = 60\,J/K/m/s$.

The case studied in this section concerns cooling effectiveness, quantified here by an expression identifying and penalizing areas with high temperatures. To do so without using non-differentiable expressions, the following sigmoid function is evaluated

$$\boldsymbol{J_T} = \int_{\boldsymbol{\Omega_S}} \boldsymbol{j_T}\, \boldsymbol{d\Omega} \tag{15}$$

where

$$j_T = \begin{cases} \left[1 - \frac{1}{1+e^{k_2(T^S - T_2)+k_1}}\right], if\ \ T^S \le T_2 \\ \alpha(T^S - T_2) + \beta, \qquad if\ \ T^S > T_2 \end{cases} \tag{16}$$

and $k_1 = log\left(\frac{1}{1-f_{max}} - 1\right), k_2 = \frac{\log\left(\frac{1}{1-f_{mim}}-1\right)-k_1}{T_1 - T_2}, \alpha = \frac{k_2 e^{k_1}}{(1+e^{k_1})^2}, \beta = \frac{e^{k_1}}{1+e^{k_1}}$ with $f_{min} = 0.001$ and $f_{max} = 0.999$. $T_1$, $T_2$ are thresholds used to regulate the slope of the sigmoid, with $T_2 > T_{1,}$. For the case studied here, $T_1 = 450K$, $T_2 = 500K$. However, a minimum value of eq. (15) could be found by just eliminating the $\Omega^S$ volume. This can be circumvented, by additionally using an equality constraint preserving the initial solid volume.

Beyond the cooling effectiveness, it is usually desirable to have cooling systems with the minimum volume-averaged total pressure losses between the inlet and outlet of $\Omega^F$, given by

$$J_{pt} = -\int_{S_{F,I,O}} \left(p + 0.5 v_k^2\right) v_j n_j dS$$

As expected and also demonstrated in fig. 4 and Table 4, min. $J_T$ and min. $J_{pt}$ under constant $\Omega^S$ volume are contradictory goals and solving such a two-objective optimization could lead to the front of non-dominated solutions (Pareto front) which is beyond the scope of this study. Hence, a single-objective optimization problem is solved, in which $J_{pt}$ is minimized by imposing equality constraints on both $J_T$ and the $\Omega^S$ volume which should keep their initial values. It is obvious that a less-restrictive inequality constraint could have been used for $J_T$ by requiring it not to exceed its initial value. However, the outcome of such an optimization is expected to lead $J_T$ to its maximum allowed (i.e. the initial) value, in order to reduce $J_{pt}$ as much as possible.

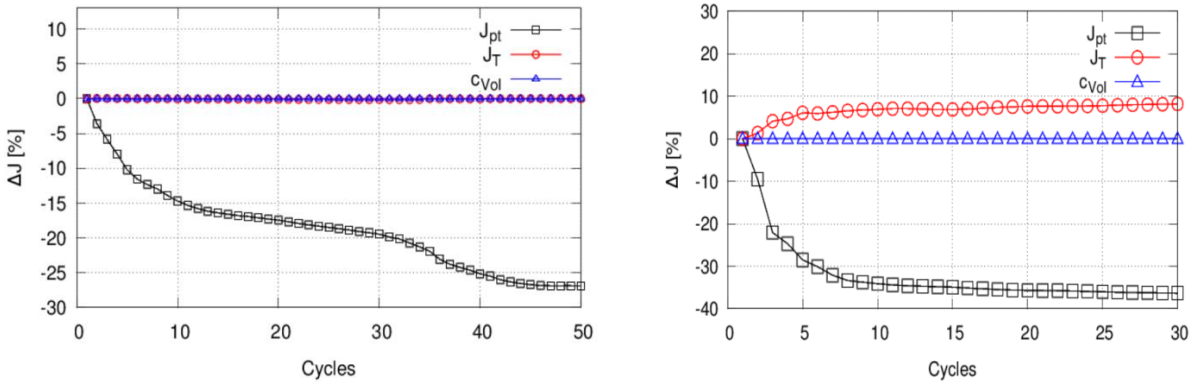


**Figure 3: Convergence of objective and constraint functions for Cases (a) on the left and (b) on the right. Note that, in Case (a) $J_T$ acts as an equality constraint whereas in (b) this is not considered during the optimization. In both diagrams, Cvol refers to the equality constraint for the $\Omega^S$ volume.**

In Table 4 the contradictory behaviour of min. $J_T$ and min. $J_{pt}$ under the volume constraint is showcased by comparing the results of two optimization case studies, (a) a first pertaining to the minimization of $J_{pt}$ under constant $J_T$ and (b) a second one regarding the minimization of $J_{pt}$ without constraining $J_T$. In both cases, the $\Omega^S$ volume equality constraint is used and convergence histories are plotted in fig 3. Case (a) satisfies the two constraints but leads to a smaller reduction in $J_{pt}$ compared to (b), in which $J_T$ has increased by $\sim 8\%$ compared to the initial one. This is due to the fact that, in order to reduce $J_{pt}$, velocity magnitudes are decreased, see fig. 4, deteriorating thus heat convection and inevitably leading to higher $T^S$ and $J_T$. On the contrary, in Case (b), focusing exclusively on $J_{pt}$, heat conduction between the solid and the coolant is slightly reduced compared to Case (a) due to a shorter FSI length, fig. 5.

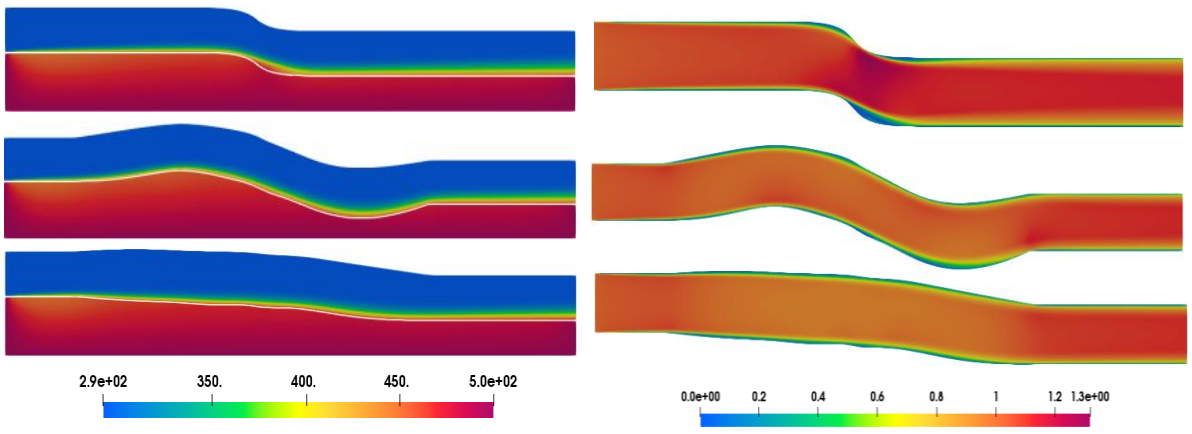


**Figure 4: Temperature (left) and velocity magnitude (right, x,y axes not in scale) fields over the baseline geometry (top) and the optimized geometries of Case a (middle) and b (bottom). In both cases, the same volume constraint is imposed.**

| Change of functions during optimization | No $J_T$ constraint | With $J_T$ constraint |
|---|---|---|
| $\Delta J_{pt}$ | -36.3% | -26.9% |
| $\Delta J_T$ | +8.2% | +0.003% |

**Table 4: Comparison between the reduction of $J_{pt}$ and change in $J_T$ between Cases (a) and (b).**

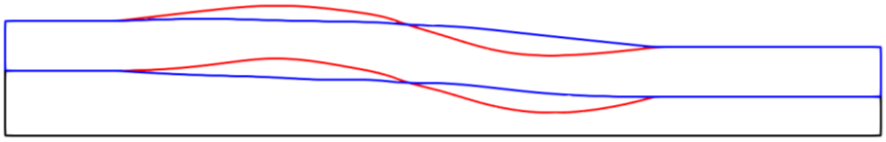

**Figure 5: Comparison between optimized geometries of Case (a) (in red) and (b) (in blue).**

## 5.2 3D optimization cases

In this section, the improvement of the cooling effectiveness of the internal cooling system of fig. 6 is studied. The geometry to be optimized comprises a 3D U-Bend cooling duct, fully placed inside a rectangular solid body. Along the non-FSI walls of $\Omega^S$, a Dirichlet temperature condition ($T^S = 400K$) is imposed. The fluid flow is turbulent ($Re = 84000$ based on the duct hydraulic diameter, average $y^+ = 0.77$ for the first barycenters off the wall), with inlet velocity of magnitude $16.8\ m/s$ being parallel to the axial direction and $T^F|_{S_{F,I}} = 288K$. Also, $c_p = 4181\ J/K/kg$, $Pr = 0.1$, $Pr_t = 1$ and $k^S = 60\ J/K/m/s$.

Two optimizations are performed: (a) minimization of $J_T$, given by eq. (15) with $T_1 = 360K$ and $T_2 = 395K$ and (b) maximization of the heat flux crossing the FSI (or, equivalently, the maximization of the heat absorbed by the coolant)

$$J_F = \int_{S^F} k^F \frac{\partial T^F}{\partial n} dS \tag{17}$$

Also, two different control boxes, namely Boxes 1 and 2, with different distances of the control box edges from the FSI, are used to parameterize the geometry (see fig. 6); in both cases, the same number of CPs ($11 \times 20 \times 9$ along the three directions) is used and the same part of the FSI is parameterized. The x,y,z coordinates of the CPs are used as design variables and for each control box, all boundary CPs are kept fixed. In both cases, the control box is fully enclosed within the solid body, keeping its outer shape fixed (fig. 6).

In Table 5, the results of the optimizations for both objective functions are summarized. It can be seen that Box 1 happens to provide comparatively better objective function values. This difference in objective values is also depicted in the optimized shapes; in fig. 7 it can be observed that changing the control box size affects the parts of the FSI that have been displaced. In specific, Box 1 mainly affects the frontal part of the U-bend while Box 2 affects more the lateral parts. By looking at figs. 8 and 9, depicting

the temperature and velocity magnitudes in the optimized geometries, it can be seen that by increasing the velocity magnitude at the top of the U-bend and at the part following the flow turning, heat convection is positively affected and thus smaller temperatures near the FSI occur, reducing thus $J_T$; a larger temperature gradient and a bigger surface of the FSI leads also to the maximization of $J_F$.

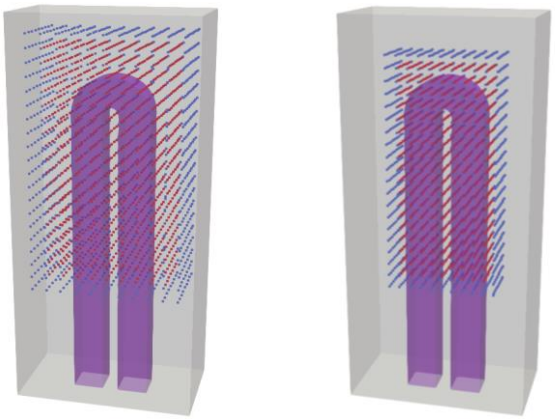

**Figure 6: Baseline geometry along with Boxes 1 (left) and 2 (right). CPs in blue are kept fixed while red ones can be displaced during the optimization. The purple surface and gray rectangle correspond to the FSI and solid outer boundary, respectively.**

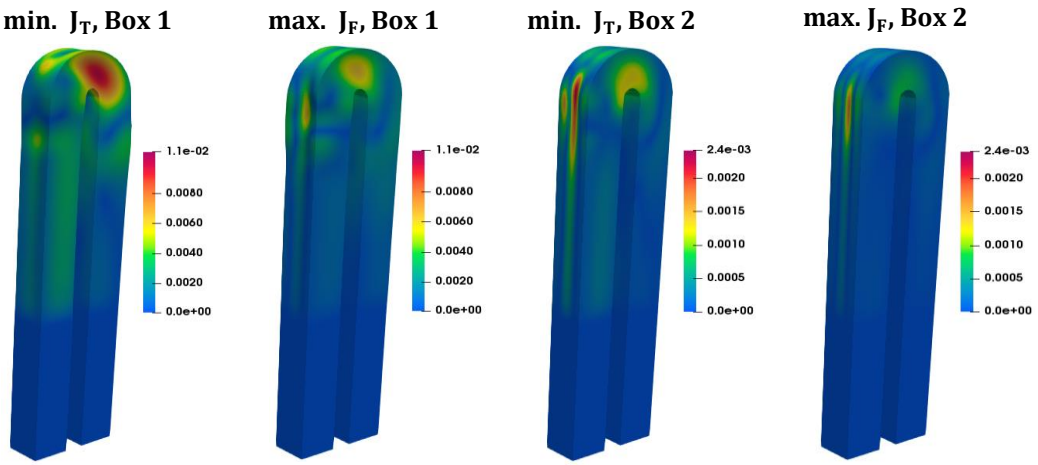


**Figure 7: Magnitude of cumulative displacement fields for min. $J_T$ and max. $J_F$ for Boxes 1 and 2.**

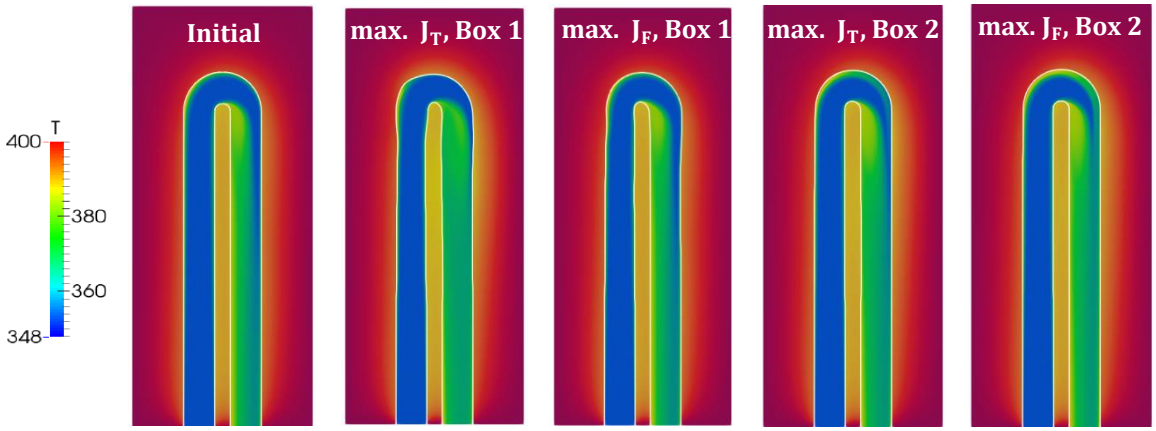


**Figure 8: Temperature fields for $\Omega^F$ and $\Omega^S$, plotted on a slice in the middle of the duct width. Initial (left) and optimized geometries (from left to right, min. $J_T$ and max. $J_F$ and for Boxes 1 and 2).**

| | Min. $J_T$ | Max. $J_F$ |
|---|---|---|
| Box 1 | -2.7% | +7.5% |
| Box 2 | -1.4% | +4.4% |

**Table 5: Results of the optimizations for the two objective functions and two control boxes.**


**Figure 9: Velocity magnitude over $\Omega^F$ for the initial (left) and optimized geometries (layout of geometries as in fig. 8).**

## 5. Conclusions

In this paper, the continuous adjoint method for CHT problems with turbulent flows, developed and presented in detail in **(10)** by the same authors, is extended for new objective functions and is used to drive an optimization algorithm based on the Armijo backtracking line-search method **(11)**. A number of shape optimization cases were studied in this paper for 2D and 3D internal cooling systems; the latter could comprise parts of the cooling systems found inside piston engines and turbine bladings. Constrained problems were examined by demonstrating that enhancing the efficiency of cooling and minimizing the volume averaged total pressure losses in the cooling channel are contradictory goals. The first of the two goals requires larger surface area between the cooled device and the coolant to improve heat conduction between them and higher velocity magnitude to improve heat convection, while the second goal is achieved when the opposite trends are followed during the design process. On the other hand, minimizing the overheated part of the solid area or maximizing the heat flux through the FSI do not lead to the same optimal solutions and is thus interesting to have both adjoint methods developed and programmed.

## Acknowledgments

The research work was supported by the Hellenic Foundation for Research and Innovation (HFRI) and the General Secretariat for Research and Technology (GSRT), under the HFRI PhD Fellowship grant (GA. no. 1796).

## References:

**1.** Dennis, B.H., et al., et al. ***Optimization of a large number of coolant passages located close to the surface of a turbine blade.*** **s.l. : ASME Paper GT2003-38051, 2003.**

**2.** Nowak, G. and Wroblewski, W. ***Cooling system optimisation of turbine guide vane.*** **s.l. : Applied Thermal Engineering, 2009. pp. 567–572. Vol. 29.**

**3.** Wang, B., et al., et al. ***Multiconfiguration shape optimization of internal cooling systems of a turbine guide vane based on thermomechanical and conjugate heat transfer analysis.*** **s.l. : Journal of Heat Transfer, 2015. Vol. 137.**

**4.** Mousavi, A. and Nadarajah, S.K. ***Heat transfer optimization of gas turbine blades using an adjoint approach.*** **s.l. : AiAA Paper 2010-9048, 2010.**

**5.** Mousavi, A. and Nadarajah, S.K. ***Adjoint-based multidisciplinary design optimization of cooled gas turbine blades.*** **s.l. : AIAA Paper 2011-1131, 2011.**

**6.** M., Ferlauto. ***An inverse method of designing the cooling passages of turbine blades based on the heat adjoint equation.*** **s.l. : Journal of Power Energy, 2014. pp. 328–339. Vol. 228.**

**7.** Willeke, S. and Verstraete, T. ***Adjoint Optimization of an Internal Cooling Channel U-Bend.*** **s.l. : ASME GT2015-43423 Turbo Expo: Power for Land, Sea, and Air, 2015. Vol. 5A: Heat Transfer.**

**8.** Verstraete, T., Mueller, L. and Mueller, J.D. ***Adjoint-Based Design Optimisation of an Internal Cooling Channel U-Bend for Minimised Pressure Losses.*** **s.l. : International Journal of Turbomachinery. Propulsion and Power., 2017. Vol. 2.**

**9.** Zeinalpour, M., Mazaheri, K. and Kiani, K. ***A coupled adjoint formulation for non-cooled and internally cooled turbine blade optimization.*** **s.l. : Applied Thermal Engineering, 2016. pp. 327-335 . Vol. 105.**

**10.** Gkaragkounis, K. T., Papoutsis-Kiachagias,, E.M. and Giannakoglou, K.C. ***The continuous adjoint method for shape optimization in conjugate heat transfer problems with turbulent incompressible flows.*** **s.l. : Applied Thermal Engineering, 2018. pp. 351–362. Vol. 140.**

**11.** Nocedal, J. and Wright, S. ***Numerical Optimization.*** **New York : Springer, 1999.**

**12.** Spalart, P. and Allmaras, S. ***A one-equation turbulence model for aerodynamic flows.*** **Reno, Nevada : AIAA Paper 1992-0439, 30th Aerospace Sciences Meeting and Exhibition, 1992.**

**13.** Papoutsis-Kiachagias, E.M.; Giannakoglou, K.C. ***Continuous adjoint methods for turbulent flows, applications.*** **s.l. : Archives of Computational Methods in Engineering, 2016. pp. 255–299 . Vol. 23.**

**14.** Zymaris, A., et al., et al. ***Continuous adjoint approach to the Spalart-Allmaras turbulence model for incompressible flows.*** **s.l. : Computers & Fluids, 2009. pp. 1528–1538. Vol. 38.**

**15.** Papoutsis-Kiachagias, E.M., et al., et al. ***Noise reduction in car aerodynamics using a surrogate objective function and the continuous adjoint method with wall functions.*** **s.l. : Computers & Fluids, 2015. pp. 223-232. Vol. 122.**